JTTEE5 7:205-212

PEER REVIEWED

Gas Dynamic Principles of Cold Spray

R.C. Dykhuizen and M.F. Smith

(Submitted 10 September 1997; in revised form 9 March 1998)

This paper presents an analytical model of the cold-spray process. By assuming a one-dimensional isentropic flow and constant gas properties, analytical equations are solved to predict the spray particle velocities. The solutions demonstrate the interaction between the numerous geometric and material properties. The analytical results allow determination of an optimal design for a cold-spray nozzle. The spray particle velocity is determined to be a strong function of the gas properties, particle material density, and size. It is also shown that the system performance is sensitive to the nozzle length, but not sensitive to the nozzle shape. Thus, it is often possible to use one nozzle design for a variety of operational conditions. Many of the results obtained in this article are also directly applicable to other thermal spray processes.

Keywords analytic, coating, cold spray, gas dynamic

1. Introduction

Cold-spray processing (or simply cold spray) is a high-rate material deposition process in which small, unmelted powder particles (typically 1 to 50 μm in diameter) are accelerated to velocities on the order of 600 to 1000 m/s in a supersonic jet of compressed gas. Upon impact with a target surface, the solid particles deform and bond together, rapidly building up a layer of deposited material (Fig. 1). Cold spray was developed in the mid-1980s at the Institute of Theoretical and Applied Mechanics of the Siberian Division of the Russian Academy of Science in Novosibirsk (Ref 1, 2). While performing supersonic wind tunnel tests with flows containing small tracer particles, scientists observed that above a critical particle velocity (which varies for different materials) there was a transition from particle erosion of a target surface to rapidly increasing deposition (Fig. 2). Although this wind tunnel phenomenon had been observed by others, the Russians developed the process as a coating technology. They successfully deposited a wide range of pure metals, metal alloys, polymers, and composites onto a variety of substrate materials. They also demonstrated that cold spray can rapidly apply coatings over large surface areas, ranging up to 5 m^2/min (~300 ft^2/min) in a pilot demonstration system for cold-spray coating of pipe. A U.S. patent was issued in 1994 (Ref 1).

In the United States, further research has been conducted by a consortium of companies organized under the auspices of the National Center for Manufacturing Sciences (Ref 4, 5). These investigators have used the term cold gas dynamic spray method (CGSM) for this process, but in this article, it is simply referred to as "cold spray."

Figure 3 illustrates a typical cold-spray device. Compressed gas, at device inlet pressures ranging up to 30 bar (500 psi), flows through a converging/diverging nozzle to develop supersonic gas velocities. The powder particles are metered into the gas flow immediately upstream of the converging section of the nozzle and are accelerated by the rapidly expanding gas. The incoming compressed gas can be introduced at room temperature, or it can be preheated in order to achieve higher gas flow velocities in the nozzle. Although preheat temperatures as high as 900 K (1200 °F) are sometimes used, the gas rapidly cools as it expands in the diverging section of the nozzle. Hence, the dwell time of the particles in contact with hot gas is brief, and the temperatures of the solid particles at impact remain substantially below the initial gas preheat temperature.

The actual mechanisms by which the solid-state particles deform and bond has not been well characterized. It seems plausible, though it has not yet been demonstrated, that plastic deformation may disrupt thin surface films, such as oxides, and provide intimate conformal contact under high local pressure,

R.C. Dykhuizen and **M.F. Smith,** Sandia National Laboratories, Albuquerque, NM 87185-0835. Contact e-mail: rcdykhu@sandia.gov.

Nomenclature

A	Cross-sectional flow area of the nozzle
A_p	Cross-sectional area of the particle
C_D	Drag coefficient
C_p	Gas heat capacitance at constant pressure
D	Drag force on a particle
$\dot{m}$	Mass flow rate
M	Mach number
m	Mass of the particle
P	Pressure
R	Specific gas constant
T	Temperature
V	Gas velocity
V_p	Particle velocity
x	Axial position
X	Nondimensional axial position
ρ	Gas density
γ	Ratio of gas specific heats

Subscripts and superscripts

*	Nozzle throat conditions
e	Nozzle exit conditions
p	Particle conditions
s	Postshock conditions

thus permitting bonding to occur. Though unproven, this hypothesis is consistent with the fact that a wide range of ductile materials, such as metals and polymers, have been cold-spray deposited. However, experiments with nonductile materials, such as ceramics, have not been successful unless they are codeposited along with a ductile matrix material. This theory would also explain the observed minimum critical velocity necessary to achieve deposition, because sufficient kinetic energy must be available to plastically deform the solid material. Calculations indicate that the particle kinetic energy at impact is typically much less than the energy required to melt the particle. Micrographs of cold-sprayed materials, such as Fig. 4, also suggest that the deposition mechanism is primarily, and perhaps entirely, a solid-state process.

Because particle velocity is so critical to successful cold-spray deposition, it is important to develop a sound understanding of the relative influence of process variables, such as gas inlet pressure and temperature and nozzle geometry, on particle velocity. It is hoped that the analytical expressions, computational results, and discussions presented in this article will help to foster an increased understanding of the cold-spray process and may also serve to enhance understanding of other closely related thermal spray processes.

1.1 Potential Cold-Spray Advantages and Limitations

Because cold spray does not use a high-temperature heat source, such as a flame or plasma, to melt the feed material, it does not deposit large amounts of heat into a coated part, nor does it degrade thermally sensitive coating materials through oxidation or other inflight chemical reactions. For this reason, cold spray seems very attractive for depositing oxygen-sensitive materials, such as copper or titanium. Similarly, cold spray offers exciting new possibilities for building thick coatings, and even free-standing shapes, from nanophase materials, intermetallics, or amorphous materials. These materials are often difficult to spray using conventional thermal spray techniques.

The cold-spray process often allows avoidance of grain growth and the formation of brittle phases. Cold spray also may

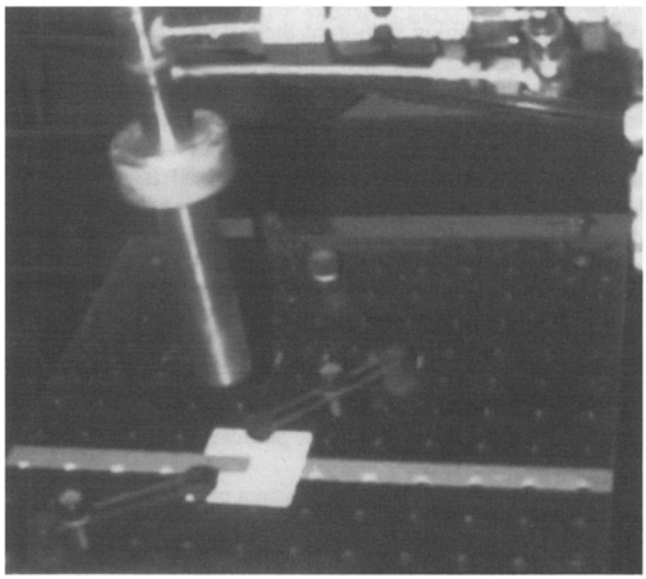

Fig. 1 Copper being cold-spray deposited directly onto an unprepared surface of a square aluminum oxide wafer with Sandia National Laboratories new cold-spray system

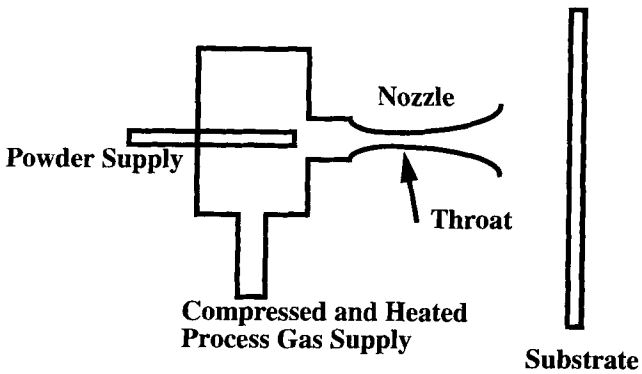

Fig. 3 Typical cold-spray system geometry

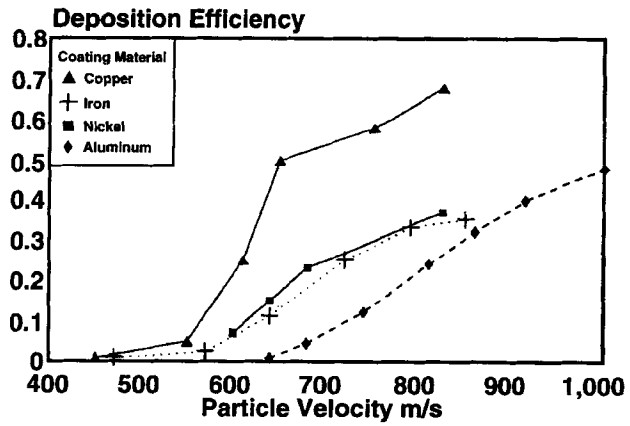

Fig. 2 Deposition efficiency versus particle velocity (Ref 3)

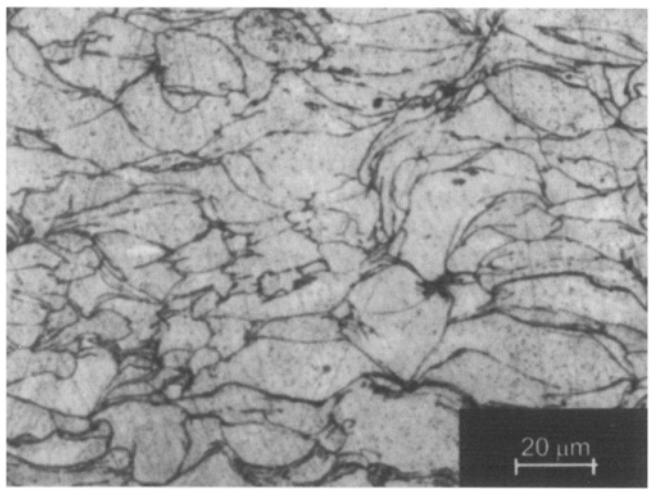

Fig. 4 Micrograph of an etched cold-sprayed steel coating. The sharp, angular features observed suggest plastic deformation upon impact and, at this magnification, there is no indication of local melting. (In unetched specimen the boundaries are not visible.)

prevent chemical segregation that can occur during solidification. For example, titanium aluminide has a very attractive strength to weight ratio. However, efforts to produce titanium aluminide hardware by conventional melting/forming technologies have met with only limited success due to macro- and microsegregation of alloying elements during solidification. The best properties are only achieved in atomized powders. Cold spray of these powders may make it possible to achieve those same desirable properties in bulk materials.

Another potential advantage is that residual tensile stresses associated with solidification shrinkage are eliminated. In fact, it has already been demonstrated that the "peening" effect of the impinging solid particles can produce potentially beneficial compressive residual stresses in cold-spray deposited materials (Ref 4). Cold spray may also offer advantages for some combinations of dissimilar materials. For example, aluminum can be cold-spray deposited directly onto a smooth, unprepared glass surface. Cold-spray deposition of materials such as copper, solder, and polymeric coatings may also provide a cost-effective "green" alternative to technologies such as electroplating, soldering, and painting (Ref 6).

As with other spray technologies, one important limitation of cold spray is that it is a line-of-sight process. In addition, not all materials can be cold-spray deposited. As indicated earlier, ceramics and other nonductile materials do not seem amenable to this process. For materials that are cold-spray compatible, the data in Fig. 2 show that deposition efficiency is strongly dependent on particle velocity. Achieving high-particle-impact velocities with very dense materials, such as tungsten or other refractory metals, can also pose significant challenges.

2. Model Equations

This section presents the model equations. First, the gas flow model is introduced. It is assumed that the gas flow conditions can be calculated without consideration to feedback from the powder flux. Then the powder flow model is introduced. From the powder flow solution, optimal conditions are identified that yield maximum powder acceleration. Next, equations are introduced that describe the nozzle shape that yields the optimal condition. Finally, the particle velocity for the optimal nozzle is analytically determined.

2.1 Isentropic Gas Flow Model

The spray particle velocity that can be obtained via a cold-spray device is limited only by the gas velocity. Use of a high-pressure gas flow, long nozzles, and small particles results in particles traveling at the gas velocity. The gas velocity can be increased by using low molecular weight gases, high temperatures, and large expansion ratio nozzles. However, practical limits exist for all of the process variables. Thus, it is desirable to produce a sufficient spray particle velocity, with an optimal design, so that the guns can be compact and the gas use minimized. It is also desirable to avoid using high gas pressures and temperatures. The analytic equations presented in this article allow the design of such a device.

The typical cold-spray geometry includes a converging/diverging nozzle, which is shown schematically in Fig. 3. It is assumed that the gas flow is isentropic (adiabatic and frictionless) and one dimensional. It is also assumed that the process gas can be approximated as a perfect gas with constant specific heats. Thus, the applicable gas flow equations can be obtained from any classical text on fluid flow (e.g., Ref 7, 8), and analytical solutions are possible. The one-dimensional analysis ignores the small gas flow boundary layers along the nozzle walls, where the gas is traveling slower than the mean. Thus, the gas flow rates calculated by the model are slightly higher than those obtained in practice. Also, the one-dimensional assumptions limit the application of the model to regions away from the jet impingement on the substrate.

The above assumptions yield gas conditions that are a function of the nozzle geometry, total gas temperature, and stagnation pressure. The flow is accelerated or decelerated by changing flow areas. The total gas temperature and stagnation pressure are those that would be measured at the source of the gas, where it is stagnant. As the gas is accelerated through the nozzle, the temperature and pressure decrease from these values while the velocity increases (although the stagnation values would be reestablished if the gas were isentropically decelerated to zero velocity). The gas conditions for this type of problem are typically written as a function of the local Mach number (the velocity of the gas divided by the local sound speed). However, the local flow area and the local Mach number can be related. The optimal variation of the local flow area with axial distance (the shape of the nozzle) is one of the outputs that can be obtained from the analysis presented here.

It is interesting to examine briefly the thermal aspects of the cold-spray process. Typically, the total temperature of a cold-spray gas is hotter than ambient. This produces improved performance via greater gas velocities. The higher-temperature gas causes the spray particles to heat up as they encounter the gas stream. However, as the gas gains kinetic energy, it cools. If the spray particle does not accelerate quickly, the gas temperature it experiences will remain constant because the gas has to slow back down to interact with the static particle. However, as the particle approaches the gas velocity, the thermal energy transfer is now with a cool gas and often results in cooling the spray particle. Numerical simulation of this process shows that the particle interacts with the slow warm gas for greater time periods and with higher heat transfer coefficients than with the fast cool gas, so the net effect is a slightly elevated-temperature spray particle upon impact. No further discussion of the thermal aspects of cold spray is provided in this article. However, it is noted here that the particle flux is assumed to be dilute so that any heat transfer between the particles and gas does not violate the adiabatic gas flow assumption.

The process gas flow is assumed to originate from a large chamber or duct where the pressure is equal to the stagnation pressure (P_0), the temperature is the total temperature (T_0), and the velocity is zero. For practical purposes, this matches the conditions upstream of the nozzle throat where the flow area is greater than three times the throat area.

It is assumed that the total temperature and the mass flow rate (not the stagnation pressure) is set by the user. The mass flow rate is frequently set in thermal spray devices by setting a pressure level upstream of a critical flow orifice in the gas supply line. Note that this pressure is not equal to the stagnation pres-

sure of the flow through the nozzle because of the frictional losses associated with the gas traversing the orifice.

The following equation relates the gas temperature at the throat (T^*)to the total gas temperature (note all quantities given with an * are throat or sonic conditions):

$$\frac{T_o}{T^*} = 1 + \frac{\gamma - 1}{2} \quad \text{(Eq 1)}$$

where γ is the ratio of specific heats. For monatomic gases, γ is 1.66, and for diatomic gases γ is typically 1.4. (Air is typically modeled as a diatomic gas because it is a mixture of nitrogen and oxygen.) Larger molecules have even lower specific heat ratios, but are typically not used in thermal spray applications.

Equation 1 assumes that the throat condition is sonic. Sonic conditions are only obtained for sufficient stagnation gas pressures, but this condition is usually obtained for all thermal spray applications. At the throat, the Mach number is unity, and the local velocity can be obtained from:

$$V^* = \sqrt{\gamma R T^*} \quad \text{(Eq 2)}$$

where R is the specific gas constant (the universal gas constant divided by the gas molecular weight). Equation 2 illustrates why it is often found that helium makes a better carrier gas due to its smaller molecular weight and higher specific heat ratio.

A mass balance yields the throat density:

$$\rho^* = \frac{\dot{m}}{V^* A^*} \quad \text{(Eq 3)}$$

At this point, the throat area (A^*) can be set to unity and the mass flow rate ($\dot{m}$) specified as a flux per unit throat area. This allows obtaining a single solution that can then be easily scaled by the throat area if desired.

Using the perfect gas law, the throat pressure is obtained:

$$P^* = \rho^* R T^* \quad \text{(Eq 4)}$$

From the throat pressure, the stagnation pressure can be calculated:

$$\frac{P_o}{P^*} = \left(1 + \frac{\gamma - 1}{2}\right)^{\gamma/(\gamma-1)} \quad \text{(Eq 5)}$$

If sonic conditions are to be maintained at the throat, the throat pressure must be above the ambient, or spray chamber, pressure.

To complete the gas dynamic calculation, a single nozzle exit condition needs to be specified. This could be the exit pressure, exit velocity, exit Mach number, or exit area. The gas exit pressure need not match the ambient pressure. Current cold-spray gun operating conditions have an exit pressure well below ambient to obtain maximum spray particle velocities. Thus, the gas flow is said to be overexpanded. This results in a flow outside of the nozzle that cannot be solved by simple one-dimensional gas dynamic equations. However, the one-dimensional results presented here still apply inside the nozzle as long as the overexpansion is not so great as to cause a normal shock inside the gun. Shocks inside the gun have not been predicted in operational conditions tested at Sandia to this point.

It is assumed here that the exit area is specified. The following equation is used to obtain the exit Mach number when the exit area is specified:

$$\frac{A}{A^*} = \left(\frac{1}{M}\right)\left[\left(\frac{2}{\gamma+1}\right)\left(1 + \frac{\gamma-1}{2} M^2\right)\right]^{(\gamma+1)/[2(\gamma-1)]} \quad \text{(Eq 6)}$$

With the exit Mach number known, the other gas conditions can be obtained from the following isentropic relationships:

$$\frac{P}{P^*} = \left(\frac{\gamma+1}{2 + (\gamma-1) M^2}\right)^{\frac{\gamma}{(\gamma-1)}} \quad \text{(Eq 7)}$$

$$\frac{T_o}{T} = 1 + \frac{\gamma - 1}{2} M^2 \quad \text{(Eq 8)}$$

$$V = M\sqrt{\gamma R T} \quad \text{(Eq 9)}$$

$$\frac{\rho_o}{\rho} = \left(1 + \frac{\gamma - 1}{2} M^2\right)^{1/(\gamma-1)} \quad \text{(Eq 10)}$$

Because the exit pressure calculated is typically less than ambient, a simple check is required to make sure the given solution is possible. The following calculation yields a trial pressure for the design. P_s is the downstream shock pressure that would be obtained if a shock occurred at the nozzle exit:

$$\frac{P_s}{P_e} = \frac{2\gamma}{\gamma+1} M_e^2 - \frac{\gamma-1}{\gamma+1} \quad \text{(Eq 11)}$$

If this pressure (P_s) is equal to the ambient pressure, a shock occurs at the nozzle exit. If this pressure is less than the ambient pressure, a shock occurs somewhere inside the nozzle, and subsequent subsonic flow occurs past the shock location so that the exit pressure is equal to the ambient pressure. The normal operating condition for cold-spray nozzles results in the exit pressure being less than the ambient pressure, and P_s being greater than the ambient pressure. When this is the case, the flow is overexpanded and all conditions calculated represent real conditions inside of the nozzle. The gas stream then slows down outside of the nozzle exit as the pressure adjusts to the ambient. This gas deceleration upon exiting is not as significant in cold-spray applications as in other thermal spray processes due to the short standoff distances.

Equations 1 through 4 and 6 through 10 can also be used to simulate plasma or HVOF spray systems by assuming an isentropic expansion from the throat to the exit of a diverging nozzle. However, the total gas temperature must be obtained through an energy balance. The total gas temperature is greater than the incoming gas temperature due to the energy additions. So, in place of Eq 5 (to calculate the stagnation pressure), another relation must be substituted. Reasonable agreement with experimental data has been obtained using a Rayleigh Line calculation instead of the isentropic assumption (Ref 9, 10). The Rayleigh Line calculation assumes a constant area energy addition.

2.2 Particle Acceleration Model

It is not the gas conditions that determine the adequacy of the cold-spray process, but the spray particle velocity. In this section the acceleration of the particles is considered. It is assumed that the two-phase flow (gas and particles) is dilute enough so that the above equations hold. This has proven to be a reasonable assumption in earlier studies (Ref 9, 10). The acceleration of the particle velocity can be equated to the drag force on the particle:

$$m\frac{dV_p}{dt} = mV_p\frac{dV_p}{dx} = \frac{C_D A_p \rho (V - V_p)^2}{2} \qquad \text{(Eq 12)}$$

From Eq 12, it is seen that the ultimate spray particle velocity is equal to the gas velocity. This yields an interesting conclusion. It is shown by Eq 6, 8, and 9 that the gas velocity within the nozzle is a function only of the total gas temperature and the nozzle geometry. Thus, the gas pressure does not affect the gas velocity. However, examination of Eq 9, 10, and 12 shows that the initial drag on the particle (or the particle acceleration) is linearly dependent only on the stagnation pressure and is independent of the total temperature. Thus, the pressure has to be sufficient to allow the particle to approach the gas velocity in a finite distance.

Equation 12 can be integrated if the gas velocity and density are held constant, and the drag coefficient is assumed constant (later models presented consider a variable drag coefficient):

$$\log\left(\frac{V - V_p}{V}\right) + \frac{V}{V - V_p} - 1 = \frac{C_D A_p \rho x}{2m} \qquad \text{(Eq 13)}$$

For low values of the spray particle velocity (as compared to the gas velocity), Eq 13 can be simplified:

$$V_p = V\sqrt{\frac{C_D A_p \rho x}{m}} \qquad \text{(Eq 14)}$$

This yields the simple relationship where the spray particle velocity is proportional to square root of the distance traveled over the particle diameter (Ref 11). It also shows the importance of large gas densities.

2.3 Optimal Particle Acceleration

Examination of Eq 12 through 14 shows that the acceleration of a particle increases with increasing gas velocity and increasing gas density. However, the gas dynamic equations reveal that the gas density decreases as the gas velocity increases through the supersonic nozzle. Thus, there exists an optimal condition that yields a maximum acceleration. This optimal condition can be obtained by determining a maximum drag force on the particle (i.e., the right-hand side of Eq 12). It is assumed that the particle velocity is small compared to the gas velocity. The maximum is found by differentiating the right-hand side of Eq 12 with respect to pressure (or temperature for they are related via the isentropic assumption) and using the perfect gas laws for the gas properties. Note that both the gas density and the gas velocity are dependent on the pressure level to which the gas is expanded.

$$D = C_D A_p (\rho V^2/2)$$

$$\frac{dT}{dP} = \frac{RT}{PC_p} \qquad \text{(Eq 15)}$$

$$\frac{dD}{dP} = C_D A_p \left(\frac{M^2}{2} - 1\right)$$

Equation 15 shows that a relative gas velocity of Mach$\sqrt{2}$ yields the optimal gas density and gas velocity that maximizes the spray particle acceleration. This result has been experimentally verified where particles were injected into a high-velocity gas stream. Figure 5 shows data obtained from a plasma spray experiment where the spray chamber pressure was varied to vary the gas Mach number downstream of the nozzle exit. The particles were injected near the nozzle exit plane, and the particle velocity was then measured as a function of the spray chamber pressure at two axial locations. The data show a maximum particle velocity near a calculated Mach number of $\sqrt{2}$, which verifies the above analysis. To simplify the analytical analysis, a Mach number of 1 is used to approximate the point where the drag is a maximum.

Of course, it is impossible to maintain a Mach 1 relative velocity throughout the cold-spray process because the particles are introduced into the subsonic portion of the flow. However, the optimal cold gas spray nozzle would quickly accelerate the gas to near Mach 1 and then continue to accelerate the gas as the particles are accelerated to maintain a Mach 1 relative velocity.

2.4 Optimal Nozzle Shape

The previous section shows that it is desirable to maintain the relative velocity between the gas and the particle near Mach 1. This results in maximum acceleration of the particle. This section develops equations that allow determination of an optimal cold-spray nozzle geometry given the spray particle properties, gas stagnation pressure, and total gas temperature. In the follow-

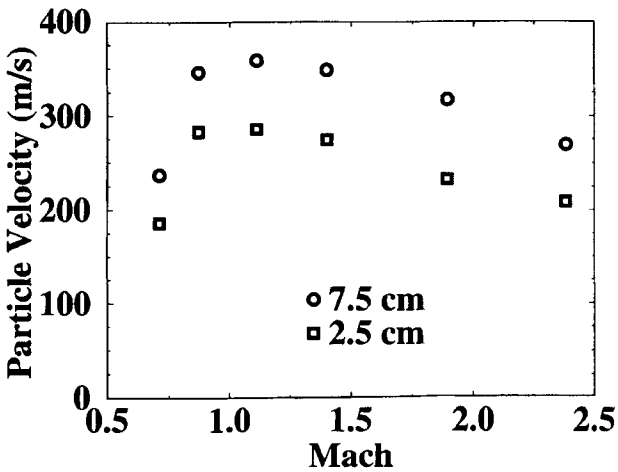

Fig. 5 Plasma spray particle velocity, at two distances from the gun exit, as a function of Mach number

ing algebraic equation the right-hand side represents a Mach 1 relative velocity:

$$V - V_p = \sqrt{\gamma RT} \qquad \text{(Eq 16)}$$

With the eventual goal of obtaining the optimal shape of the nozzle, Eq 16 is differentiated with respect to the axial position:

$$\frac{dV}{dx} - \frac{dV_p}{dx} = \frac{\sqrt{\gamma RT}}{2T}\frac{dT}{dx} \qquad \text{(Eq 17)}$$

The first term on the left-hand side of Eq 17 can be replaced by differentiation of Eq 9. The second term on the left-hand side of Eq 16 is replaced by combining Eq 12 and 16, which yields:

$$\frac{dV_p}{dx} = \frac{\gamma RTC_D A_p \rho}{(V - \sqrt{\gamma RT})2m} \qquad \text{(Eq 18)}$$

Also, the temperature derivative introduced in Eq 17 is obtained by differentiation of Eq 8. Equation 10 is used to express the local density in terms of the local Mach number. It is again assumed that the drag coefficient is constant. With some algebra, the equation set yields the following first-order differential equation for the Mach number variation.

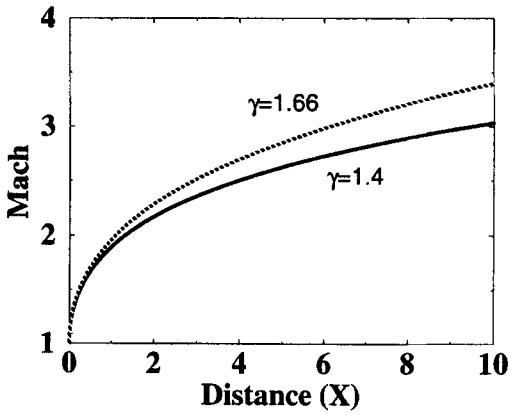

Fig. 6 Nondimensional optimal nozzle design for two specific heat ratios. Distance is measured from the throat.

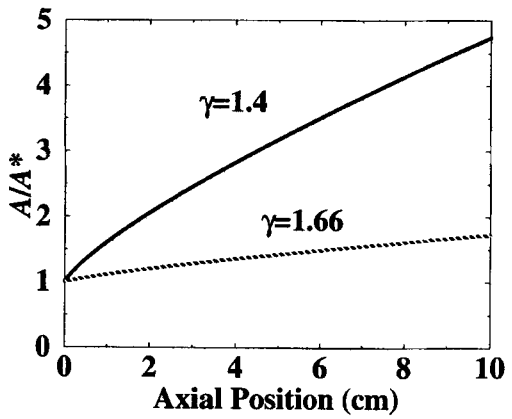

Fig. 7 Dimensional optimal nozzle designs for two specific heat-capacity ratios and specified stagnation and spray particle properties. Position is measured from the throat.

$$\frac{dM}{dX}\left(\frac{2+(\gamma-1)M}{2+(\gamma-1)M^2}\right)(M-1) = \left(\frac{2+(\gamma-1)M^2}{2}\right)^{-1/(\gamma-1)}$$

$$X = \frac{xC_D A_p \rho_o}{2m} \qquad \text{(Eq 19)}$$

Analytical solutions to Eq 19 were not found. Therefore, Eq 19 is presented in a nondimensionalized form to enable easy graphical presentation of the results. The distance (x) (and in nondimensional form X) is measured from the particle injection point, or the throat. The nondimensionalization is a function of the gas molecular weight, the gas stagnation pressure, and total gas temperature via the stagnation density (ρ_o). Thus, changing the stagnation conditions changes the optimal nozzle geometry. The optimal nozzle design is also a function of the particle material density and size via the particle cross-sectional area and mass.

The solution of Eq 19 yields (within the approximations) an optimal nozzle design. However, the design, in one aspect, is not practical. In a real application, a properly designed converging section is required to enable the isentropic flow condition assumed. However, the analytical optimal solution is a zero length converging section to obtain the required Mach 1 relative velocity as soon as possible. This is followed by a gradual expansion at such a rate as to maintain the Mach 1 relative velocity. Therefore, the solution, in a practical sense, is not the optimal one, because a gradual converging section is required to maintain the desired isentropic flow conditions. However, the solution obtained provides a starting point for a more detailed experimental or numerical determination of an optimal nozzle.

In Eq 19, the only parameter is the specific heat ratio, and only two values of the parameter are of most importance for the thermal spray community (1.4 and 1.66). Figure 6 shows the optimal solution obtained numerically.

To best display the nozzle shape results, a typical operating condition was chosen: 22 bar, 600 K, 10 μm spray particles of 8 g/cm^3 density, and a drag coefficient of unity. Using these properties, a dimensional representation of the nozzle shape can be obtained for both helium and air as the process gas (Equation 6 is used to obtain the nozzle shape as a function of position from

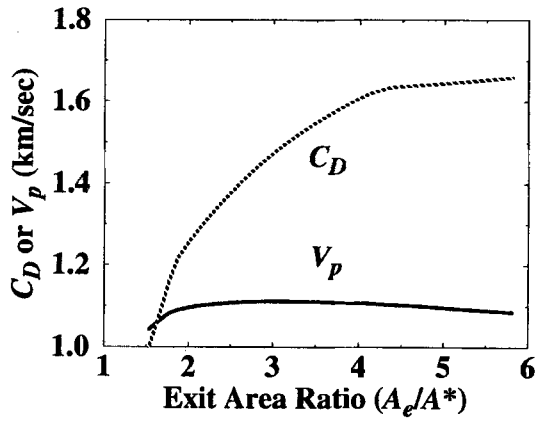

Fig. 8 Comparison of particle exit velocity and exit drag coefficient as a function of nozzle expansion ratio near the optimal solution for helium gas as determined numerically

the Mach number solution). The nozzle shape results are plotted in Fig. 7. Note that the helium nozzle (which has a lower density) expands more slowly due to the scaling shown in Eq 19.

The optimal nozzle design continues to expand indefinitely because the equations do not specify a length. The optimal shape for a finite length is simply the shape provided in Fig. 7 up to the length specified. However, if the length is extended too far, a normal shock will occur if the spray chamber pressure is held constant. (In fact, for the given conditions the air nozzle is limited to an area ratio of about 12 to 1, if sprayed into a 1 atm chamber, to prevent the occurrence of a shock.) Thus, if a longer nozzle is desired, the nozzle area would have to remain constant after this limiting value is reached, or else the flow will change to subsonic conditions after the shock. Further discussion on the effects of a shock on the nozzle design are provided later in this article.

To test the optimal results obtained, both optimal nozzles shown in Fig. 7 were input into a computer code that calculates gas and spray particle conditions. This code accounts for changing drag coefficients, but in all other aspects it is identical to the analytical model presented here. Table 1 shows the results obtained for the spray particle velocity at the exit of the nozzle. The results show that the use of helium results in higher particle velocities, as expected. It is also shown that the drastic change in the nozzle from the optimal air design to the optimal helium design makes little difference in the calculated exit particle velocity. Thus, it has been demonstrated by these, and other, simulations that the exiting particle velocity is not sensitive to the nozzle shape (although the particle velocity is shown to be sensitive to the nozzle length). The velocity is insensitive to nozzle shape because increasing the flow area of the nozzle results in faster gas velocities, but at a cost of lower gas densities. These changes tend to cancel each other for conditions near the optimal design.

When the optimal solutions (Fig. 7) are modified, it is found that they do not yield the maximum exit particle velocity, for geometries can be found that yield slightly higher results. In fact, it is shown in Table 1 that the optimal air nozzle results in faster particle velocities when helium is used than in the so-called optimal helium design. This apparent contradiction is due to the assumption of a constant drag coefficient used in the analytical model. Table 1 shows that the exit drag coefficient varies between simulations. Examination of the detailed output of the numerical model shows that the drag coefficient typically changes by 50% as a particle traverses the nozzle. Correlations in the numerical code express the drag coefficient as a function of the Reynolds number and the Mach number (Ref 12), which are a function of the changing gas temperature and the relative velocity.

Figure 8 shows how the numerically calculated exit particle velocity changes as the nozzle expansion ratio changes near the optimal solution for helium. The analytical analysis resulted in an optimal expansion ratio of 1.7 (10 cm length for a specific heat ratio of 1.66 on Fig. 7). However, the analytical analysis assumed that the drag coefficient was constant, and Fig. 8 shows that the numerically determined exit drag coefficient is not constant. The drag coefficient increases with increasing area ratio near the optimal solution. Thus, the numerically determined optimum is shown to be shifted to a slightly higher expansion ratio to take advantage of the increased drag at higher Mach numbers. Figure 8 also illustrates that the exit particle velocity is not strongly dependent on the expansion ratio, so use of the less accurate analytically determined optimal nozzle does not result in a significant reduction in the spray particle exit velocity.

2.5 *Analytical Particle Velocity*

To complete the model, the spray particle velocity is analytically determined. The exiting velocity is of most importance to the design of the cold-spray system because the coating properties are sensitive to the spray particle impact velocity. Only when the optimal nozzle shape is used can Eq 16 be used to calculate the particle velocity from the gas velocity. Then the exit Mach number for a given length nozzle is obtained from the solution to Eq 19, which is graphically presented in Fig. 6. With Eq 8, 9, and 16, the particle velocity is then expressed as a function of the gas Mach number:

$$V_p = (M - 1)\sqrt{\frac{\gamma R T_o}{1 + [(\gamma - 1)/2]M^2}} \qquad \text{(Eq 20)}$$

For illustrative purposes, Eq 20 yields a maximum particle velocity of 610 m/s for a 10 cm length nozzle using air, and 1060 m/s for the same length nozzle using helium (all with a 600 K total gas temperature, 22 bar stagnation pressure, and 10 μm 8 g/cm^3 particles). When this is compared to the more accurate numerical results presented in Table 1, it is seen that Eq 20 is quite accurate in estimating the particle velocity. In fact, because the particle velocity is somewhat insensitive to the nozzle design, Eq 20 can be used to estimate the particle velocity for all nozzle shapes. However, the Mach number used in Eq 20 should be the optimal Mach number obtained from Fig. 6 for the specified length nozzle and not the actual exit Mach number for a particular nozzle used. If Eq 20 is used in this manner, one should check for consistency by ensuring that the calculated particle velocity is less than the gas velocity calculated with the actual nozzle shape.

Equation 20 allows estimation of the increase in the particle velocity as the nozzle length increases, because Fig. 6 shows how the Mach number (for use in Eq 20) increases as the nozzle length increases.

3. Discussion

In this section, design changes are discussed that would increase the particle velocity. The governing equations presented

Table 1 Numerical results at nozzle exit

	Air nozzle		Helium nozzle	
Gas	Velocity (V_p), m/s	Exit drag coefficient (C_D)	Velocity (V_p), m/s	Exit drag coefficient (C_D)
Air	630	1.3	560	0.8
Helium	1090	1.6	1080	1.2

show that the maximum possible spray particle velocity is the gas velocity, which can be increased by using a lower molecular weight gas or by increasing the inlet gas temperature. The equations also demonstrate how higher gas pressures and smaller particles result in quicker acceleration of the spray particles. Finally, equations are provided to define an optimal nozzle shape that provides the most rapid acceleration of the particles for specified gas and particle properties.

The equations do not specify an optimal nozzle length. Longer optimal nozzles result in higher particle velocities. So, if the particle velocities obtained are not sufficient, the nozzle can always be lengthened. As the flow area increases (as specified in Fig. 6) along the length of the nozzle, the gas pressure drops correspondingly. If the nozzle becomes too large, the decreasing pressure eventually causes a shock to form inside the nozzle, abruptly reducing the gas to subsonic velocities (see Eq 11). The analytical equations show that these shocks can be avoided by raising the stagnation pressure or by reducing the ambient pressure at the nozzle exit (e.g., spray inside a chamber maintained at a reduced pressure). However, there typically are practical operational limits to the pressure levels that can be used.

An alternate approach is to lengthen the nozzle using a slower than optimal expansion rate. In this way the flow area can be limited to below that which will form the shock. This design results in lower than optimal acceleration rates, but still provides higher particle exit velocities than does use of the same expansion ratio in a shorter nozzle. This is because the longer nozzle allows a closer approach to the gas velocity. The gas velocity, at the largest obtainable expansion ratio (without a shock), is thus the maximum particle velocity that can be obtained.

Even though lengthening the nozzle increases particle exit velocities, it requires machining and qualifying new parts. As an alternative, the identical effect can be obtained by simply using a smaller diameter particle feed. For a given gas temperature and pressure, a smaller particle has a shorter optimal nozzle design (this is shown by the scaling of Eq 19). Therefore, for a nozzle of a given length and shape, switching to smaller particles provides the same net effect as lengthening the nozzle with a slower than optimal expansion rate. Particle size reduction introduces other practical limitations. Finer powder particles often result in handling problems such as clumping due to static charges. Also, the impingement of the supersonic gas jet creates a local high-pressure region. As the particle size decreases, there comes a point below which the particles are deflected and/or decelerated immediately prior to impact.

4. Conclusions

This article provides analytical equations that can be used to estimate the gas dynamics of the cold-spray process. Equations are also presented that allow calculation of the particle velocity. It is shown how the spray particle velocity depends on particle size and density, gas stagnation pressure, total gas temperature, gas molecular weight, and nozzle shape. Use of the equations derived in this article allows determination of an optimal nozzle shape given the gas conditions, particle properties, and nozzle length. However, it is shown that the spray particle velocity is relatively insensitive to the nozzle shape. Thus, a single nozzle can be used for a variety of operational conditions.

If it is determined that higher particle velocities are required, many modifications in the process are possible. One solution is to raise the total gas temperature or reduce the gas molecular weight to increase the gas velocities. Also, three changes could be made to reduce the velocity difference between the particle and the gas. These are to increase the stagnation gas pressure by increasing the gas flow rate (which increases the gas density and the drag), reduce the spray particle size, or lengthen the nozzle. The ultimate limit of the spray particle velocity is the gas velocity, and the gas velocity cannot be increased indefinitely due to practical pressure and temperature limitations and the possible occurrence of a shock if the nozzle expands to large Mach numbers (or area ratios).

The one-dimensional isentropic assumptions used in this article allow analytical solutions that enable insight into the fluid-flow processes. Many of the equations derived can also be used, with little alteration, to examine other thermal spray techniques. However, high-temperature combustion and plasma flow fields can be even farther removed from the ideal assumptions used in this article.

Acknowledgment

Sandia is a multiprogram laboratory operated by Sandia Corporation, a Lockeed Martin Company, for the United States Department of Energy under Contract DE-AC04-94AL85000.

References

1. A.P. Alkhimov, A.N. Papyrin, V.F. Dosarev, N.I. Nesterovich, and M.M Shuspanov, "Gas Dynamic Spraying Method for Applying a Coating," U.S. patent 5,302,414, 12 April 1994
2. A.O. Tokarev, Structure of Aluminum Powder Coatings Prepared by Cold Gasdynamic Spraying, *Met. Sci. Heat Treat.*, Vol 38 (No. 3-4), 1996, p 136-139
3. A.P. Alkhimov, V.F. Kosareve, and A.N. Papyrin, A Method of Cold Gas-Dynamic Deposition, *Dokl. Akad. Nauk SSSR*, Vol 315 (No. 5), 1990, p 1062-1065
4. R.C. McCune, A.N. Papyrin, J.N. Hall, W.L. Riggs, and P.H. Zajchowski, An Exploration of the Cold Gas-Dynamic Spray Method for Several Materials Systems, *Thermal Spray Science and Technology*, C.C. Berndt and S. Sampath, Ed., ASM International, 1995, p 1-5
5. R.C. McCune, W.T. Donoon, E.L. Cartwright, A.N. Papyrin, E.F. Rybicki, and J.R. Shadley, Characterization of Copper and Steel Coatings Made by the Cold Gas-Dynamic Spray Method, *Thermal Spray Science and Technology*, C.C. Berndt and S. Sampath, Ed., ASM International, 1995, p 397-403
6. C.V. Bishop and G.W. Loar, Practical Pollution Abatement Methods for Metal Finishing, *Plat. Surf. Finish.*, Vol 80 (No. 2), 1993, p 37-39
7. A.H. Shapiro, *The Dynamics and Thermodynamics of Compressible Fluid Flow*, Ronald Press, 1953
8. R.H. Sabersky, A.J. Acosta, and E.G. Hauptmann, *Fluid Flow*, Macmillan, 1971
9. M.F. Smith and R.C. Dykhuizen, The Effect of Chamber Pressure on Particle Velocities in Low Pressure Plasma Spray Deposition, *Surf. Coat. Technol.*, Vol 34 (No. 1), 1988, p 25-31
10. R.C. Dykhuizen and M.F. Smith, Investigations into the Plasma Spray Process, *Surf. Coat. Technol.*, Vol 37 (No. 4), 1989, p 349-358
11. R.A. Neiser, J.E. Brockman, T.J. Ohern, M.F. Smith, R.C. Dykhuizen, T.J. Roemer, and R.E. Teets, Wire Melting and Droplet Atomization in a High Velocity Oxy-Fuel Jet, *Thermal Spray Science and Technology*, C.C. Berndt and S. Sampath, Ed., ASM International, 1995, p 99-104
12. C.B. Henderson, Drag Coefficients of Spheres in Continuum and Rarefied Flows, *AIAA J.*, Vol 14, 1976, p 707-708